Lin_aug2010_new.qxd:JCS template2 9/1/10 8:57 AM Page 1

Application of Moment Analysis to Mass Transfer Kinetics of Reversed-Phase Liquid Chromatography: 2. A New Understanding of the External Mass Transfer Coefficient

Hong Gao[1,2,3], Xiuhong Wu[1,2], and **Bingchang Lin[1,2,*]**

[1]School of Chemical Engineering, Dalian University of Technology, Dalian, Liaoning, 116024, China; [2]Center of Separation Technology, University of Science and Technology Liaoning, Anshan, Liaoning, 114051, China; and [3]Department of Physics, Anshan Normal University, Anshan, Liaoning, 114005, China

Abstract

The second and third moments measured in the first part of this work are analyzed, combined with the moment equations deduced from the general rate model. A new understanding of the external mass transfer coefficient is obtained (i.e., the external mass transfer coefficient is linearly velocity dependent and then contributes to the intercept of the regression line of $\mu_2\mu_0^2 \sim \mu_0$). And the mass transfer parameters involved in the general rate model are also determined and discussed.

Introduction

It is well known that the resolution power of a chromatographic system mainly depends on the efficiency of the column adopted, characterized by its height equivalent to a theoretical plate. Therefore, much effort is devoted to improving column efficiency. This quest is the driving force in the continuous development of chromatographic technology.

Improving column performance requires a more fundamental understanding of the height equivalent to a theoretical plate of a column, the identification of the origin of the different contributions to this characteristic, and their proper modeling. The general rate (GR) model of chromatography provides the most powerful approach to such an investigation. This route has been taken by many authors (1–12). In this model, the different sources of band broadening are identified, modeled, and introduced in the mass balance equation of the compound considered. This partial differential equation cannot be solved for the elution band profile, but the moments of this band can be calculated as functions of the different parameters of the problem. The general solution of the problem is illustrated by the work of Miyabe et al. (2–6), who obtained some significant results on the contribution of surface diffusion. These authors compared the experimental values measured for the first and second moment to their theoretical expressions. However, the different authors following this approach had to use the Wilke-Chang (13) and the Wilson-Geankoplis correlations (14) to estimate the molecular diffusivity and the external mass transfer coefficient in order to estimate the other contributions of the mass transfer resistances to the HETP. The main imperfection of this method is that the two correlations listed earlier originated from the field of chemical engineering and were derived under sets of experimental conditions that were very different from those used in chromatography. This might introduce significant errors in the values estimated for the model parameters.

This situation reminds us of the application of higher moments, which was active in the 1970s but failed to come true because of the large measurement errors of higher moments for gas chromatographic peaks. In the first part of this work (15), it has been shown that the third moment with sufficient accuracy can be measured under proper experimental conditions for reversed-phase liquid chromatography with modern instruments and computer data acquisition and processing. The measurement result of the third central moment shows a clear regularity of the flow velocity dependence. This drives us to make further analysis about it and to obtain more fundamental information about the mass transfer kinetics in column, which cannot be acquired only from the results of the first two moments.

In the second part of the work, the measurement results of the statistical moments are analyzed, combined with the moment equations deduced from the GR model. A new understanding of the external mass transfer coefficient is obtained, and then the values of the mass transfer parameters involved in the GR model are estimated under the experimental conditions in this work.

* Author to whom correspondence should be addressed: e-mail bingchanglin@yahoo.com.

Reproduction (photocopying) of editorial content of this journal is prohibited without publisher's permission.

Lin_aug2010_new.qxd:JCS template2 9/1/10 8:57 AM Page 2

Theory

Definition of statistical moments

The n^{th} central moment (μ_n) of a chromatographic peak was defined as Eq. 1 in the first part of this work (15).

GR model

The GR model is a more complicated model because it involves the effect of nearly all possible factors that contribute to the mass transfer processes in column. Sometimes, the effect of a certain factor is weak; then it can be neglected, and this leads to the different forms of the model equations. In this work, the kinetic process of adsorption/desorption is considered to be fast enough, and its contribution to the overall process of mass transfer can be neglected. This is a reasonable assumption and has been widely used by many chromatographers. The mass balance equations and the corresponding conditions are listed as follows:

The mass balance equation for the solute in the bulk mobile phase is

$$\varepsilon_e \frac{\partial C}{\partial t} + u_0 \frac{\partial C}{\partial z} = \varepsilon_e D_L \frac{\partial^2 C}{\partial z^2} - \frac{3}{R_p}(1-\varepsilon_e) k_{ext}(C - C_p\big|_{r=R_p}) \quad \text{Eq. 1}$$

where C, C_p are the concentration of solute in the bulk and stagnant mobile phase, respectively, z is the axial coordinate along the column, r is the radial coordinate along the radius of pore in packing particles, u_0 is the superficial velocity of mobile phase ($u_0 = \frac{F}{\pi R^2}$, F is the volumetric flow rate of mobile phase and R the radius of column), ε_e is the external porosity, D_L is the axial dispersion coefficient, R_p is the average radius of the packing particles, and k_{ext} is the external mass transfer coefficient.

The initial condition of the mass balance equation is as follows:

$$C(0,z) = 0 \ (0 < z < L) \quad \text{Eq. 2}$$

where L is the length of the column.

The boundary conditions can be calculated using the following:

$$C(t,0) = \begin{cases} C_F & 0 \le t \le t_p \\ 0 & t > t_p \end{cases} \quad \text{Eq. 3}$$

$$\frac{\partial C}{\partial z}\bigg|_{z=L} = 0 \quad \text{Eq. 4}$$

where C_F is the feeding concentration of the sample of solute, and t_p is the width of the injection pulse.

The mass balance equation for the solute in the stagnant and stationary phase is

$$\varepsilon_p \frac{\partial C_p}{\partial t} + (1-\varepsilon_p)\frac{\partial q}{\partial t} = \frac{1}{r^2}\frac{\partial}{\partial r}\left(r^2\left(\varepsilon_p D_p \frac{\partial C_p}{\partial r} + (1-\varepsilon_p) D_s \frac{\partial q}{\partial r}\right)\right) \quad \text{Eq. 5}$$

where q is the concentration of solute in stationary phase, ε_p is the internal porosity, D_p is the pore diffusivity, and D_s is the surface diffusivity.

The corresponding initial conditions of the equation are

$$q(0,z,r) = 0 \quad \text{Eq. 6}$$

$$C_p(0,z,r) = 0 \quad \text{Eq. 7}$$

The natural boundary condition for the second mass balance equation at the center of pore is $\frac{\partial C_p}{\partial r}\Big|_{r=0} = 0$, and the joint condition for the two mass balance equations listed earlier at $r = R_p$ is listed below:

$$\left(\varepsilon_p D_p \frac{\partial C_p}{\partial r} + (1-\varepsilon_p) D_s \frac{\partial q}{\partial r}\right)\Big|_{r=R_p} = k_{ext}(C - C_p\big|_{r=R_p}) \quad \text{Eq. 8}$$

Because the mass transfer resistance of adsorption/desorption is neglected, the concentrations of solute in stagnant and that in stationary phase are in the state of equilibrium, and only linear adsorption isotherm is considered here ($q = GC_p$, where G is the linear adsorption constant of the adsorption isotherm); therefore, the expression of $\varepsilon_p D_p \frac{\partial C_p}{\partial r} + (1-\varepsilon_p) D_s \frac{\partial q}{\partial r}$ can be simplified as follows:

$$\varepsilon_p D_p \frac{\partial C_p}{\partial r} + (1-\varepsilon_p) D_s G \frac{\partial C_p}{\partial r} = (\varepsilon_p D_p + (1-\varepsilon_p) D_s G)\frac{\partial C_p}{\partial r} = D_{eff}\frac{\partial C_p}{\partial r} \quad \text{Eq. 9}$$

where D_{eff} is the effective diffusivity of solute:

$$D_{eff} = \varepsilon_p D_p + (1-\varepsilon_p) D_s G \quad \text{Eq. 10}$$

The analytical solution of the GR model cannot be obtained, but the moment equations of GR model can be deduced according to the correlations below, where $\overline{C}(p)$ is the solution of GR model in Laplace domain, and p is the Laplace transform variable.

$$M_1 = -\lim_{p\to 0} \frac{d \ln \overline{C}(p)}{dp} \quad \text{Eq. 11}$$

$$\mu_2 = \lim_{p\to 0} \frac{d^2 \ln \overline{C}(p)}{dp^2} \quad \text{Eq. 12}$$

$$\mu_3 = -\lim_{p\to 0} \frac{d^3 \ln \overline{C}(p)}{dp^3} \quad \text{Eq. 13}$$

Lin_aug2010_new.qxd:JCS template2 9/1/10 8:57 AM Page 3

The moment equations

As mentioned previously, the equilibrium adsorption is considered in this work, and so the model here is different from that used by Kucera (16). In his work, the nonequilibrium adsorption process was considered $\frac{\partial q}{\partial t} = aC_p - bq$ (instead of $q = GC_p$ here), where a and b are constants. And the results of moments cannot be applicable to the problem here through simple transformation. In addition, the important expression of the third moment is not involved in the moments equations presented by Kubin (17). All these are reasons for our calculating the moment equations. The process of calculation has no additional novelty, so it is not introduced in detail here, and it has been accomplished along the way by Kubin and Kucera. That is, firstly the solution of GR model in Laplace domain $\overline{C}(p)$ was deduced, and then the derivatives according to Eq. 11–13 were calculated. The works of Suzuki et al. (18) and Miyabe et al. (19) were also referred for the treatment of some particular problems. The considerable difficulty in the process of calculation is that calculations for some derivatives are complicated and time consuming, and this was the reason which Kubin (17) expressed for the third moment equation of being the most complicated model absent in his paper. Such calculations were done and checked by the tool MATLAB 7.1 in this work. The obtained moment equations are listed as follows:

$$M_1 = \frac{t_p}{2} + \frac{z}{u_0}\left[\varepsilon_e + (1-\varepsilon_e)J\right] \qquad \text{Eq. 14}$$

$$\mu_2 = \frac{t_p^2}{12} + z\,\frac{1-\varepsilon_e}{u_0}\left(\frac{2R_pJ^2}{3k_{ext}} + \frac{2R_p^2J^2}{15D_{eff}}\right) + z\,\frac{2\varepsilon_e D_L[\varepsilon_e + (1-\varepsilon_e)J]^2}{u_0^3} \qquad \text{Eq. 15}$$

$$\mu_3 = z\,\frac{6\varepsilon_e D_L[\varepsilon_e + (1-\varepsilon_e)J](1-\varepsilon_e)}{u_0^3}\left(\frac{2R_pJ^2}{3k_{ext}} + \frac{2R_p^2J^2}{15D_{eff}}\right) + z\,\frac{(1-\varepsilon_e)}{u_0}\left(\frac{4R_p^4}{105D_{eff}^2} + \frac{4R_p^3}{15k_{ext}\cdot D_{eff}} + \frac{2R_p^2}{3k_{ext}^2}\right)J^3 + z\,\frac{12\varepsilon_e^2D_L^2[\varepsilon_e + (1-\varepsilon_e)J]^3}{u_0^5} \qquad \text{Eq. 16}$$

where $J = \varepsilon_p + (1-\varepsilon_p)G$.

Experimental

Measurement of statistical moments

All the information about the experiments were described in detail in the first part of this work (15).

Determination of porosities of columns

Chemical

Uracil (99%, Alfa Aesar China, Tianjin, China) was used to measure the total porosities (ε_t) of columns. Nine polystyrene standards (narrow molecular weight distribution) of different molecular weight (Alfa Aesar China) were used to determine the external porosities (ε_e) of columns with HPLC-grade tetrahydrofuran (Chinese National Medicines Corporation, Shanghai, China) as solvent and washing mobile phase of them. And their molecular weight are 1300, 2500, 4000, 13,000, 25,000, 65,000, 152,000, 400,000, and 900,000, respectively.

Procedure

The external porosities (ε_e) of two columns were measured in the method reported by Guan et al. (20). The measured external porosities (ε_e) for column 1 and column 2 are 0.39 and 0.295, respectively. And then according to equation $\varepsilon_t = \varepsilon_e + (1-\varepsilon_e)\varepsilon_p$, the internal porosities (ε_p) for two columns can be calculated as 0.44 and 0.47 for column 1 and column 2, respectively.

Results and Discussions

All the moments results discussed below are the net moments, which means the extra-column effect has been removed.

Result of the second central moment

The experimental results of $\mu_2u_0^2 \sim u_0$ under different conditions are considered in this work (Figure 1). Obviously, the linear correlation between $\mu_2u_0^2$ and u_0 exists for all the results in Figure 1, which is indicated by the regression lines in Figure 1A–1E. The linear regression parameters are shown in Table I.

According to the theoretical result of the second central moment based on the GR model (Eq. 15), the theoretical correlation of $\mu_2u_0^2 \sim u_0$ can be written as below:

$$\mu_2u_0^2 = \frac{1}{12}\left(\frac{V_p}{\pi R^2}\right)^2 + 2L\varepsilon_e\gamma_2 dp\,[\varepsilon_e + (1-\varepsilon_e)J]^2 + Lu_0(1-\varepsilon_e)\left(\frac{2R_pJ^2}{3k_{ext}} + \frac{2R_p^2J^2}{15D_{eff}}\right) + L\,\frac{2\varepsilon_e\gamma_1D_m[\varepsilon_e + (1-\varepsilon_e)J]^2}{u_0} \qquad \text{Eq. 17}$$

where V_p is the volume of the sample injected into the column and in this work is always 20 µL. And the axial dispersion coefficient D_L in equation (15) has been replaced here according to the following correlation (1,21):

$$D_L = \gamma_1D_m + \gamma_2 dpu_0 \qquad \text{Eq. 18}$$

where D_m is the molecular diffusivity of solute in mobile phase, and γ_1, γ_2 the geometric constants are normally reported as 0.7 and 0.5, respectively.

In comparing Eq. 17 with the experimental results in Figure 1, it can be concluded that the band broadening due to the

Lin_aug2010_new.qxd:JCS template2 9/1/10 8:57 AM Page 4

molecular diffusion of solute in mobile phase can be neglected. The axial dispersion is mainly attributed to the eddy diffusion and then $D_L = \gamma_2 dpu_0$. This is easy to understand because of the small molecular diffusivity of solute in liquid mobile phase. And then, the values of γ_2 under different experimental conditions are obtained and presented in Figure 1A–1E, respectively. Apparently, all of them are much larger than 0.5 and lead to the axial dispersion coefficients larger than that estimated from Eq. 18, where γ_2 is equal to 0.5. In fact, this is not the first time that large axial dispersion coefficient is observed. Ruthven also pointed out (21) that in most of earlier studies, the extent of axial dispersion coefficient in the low Reynolds number region was underestimated. The problem will be further discussed later.

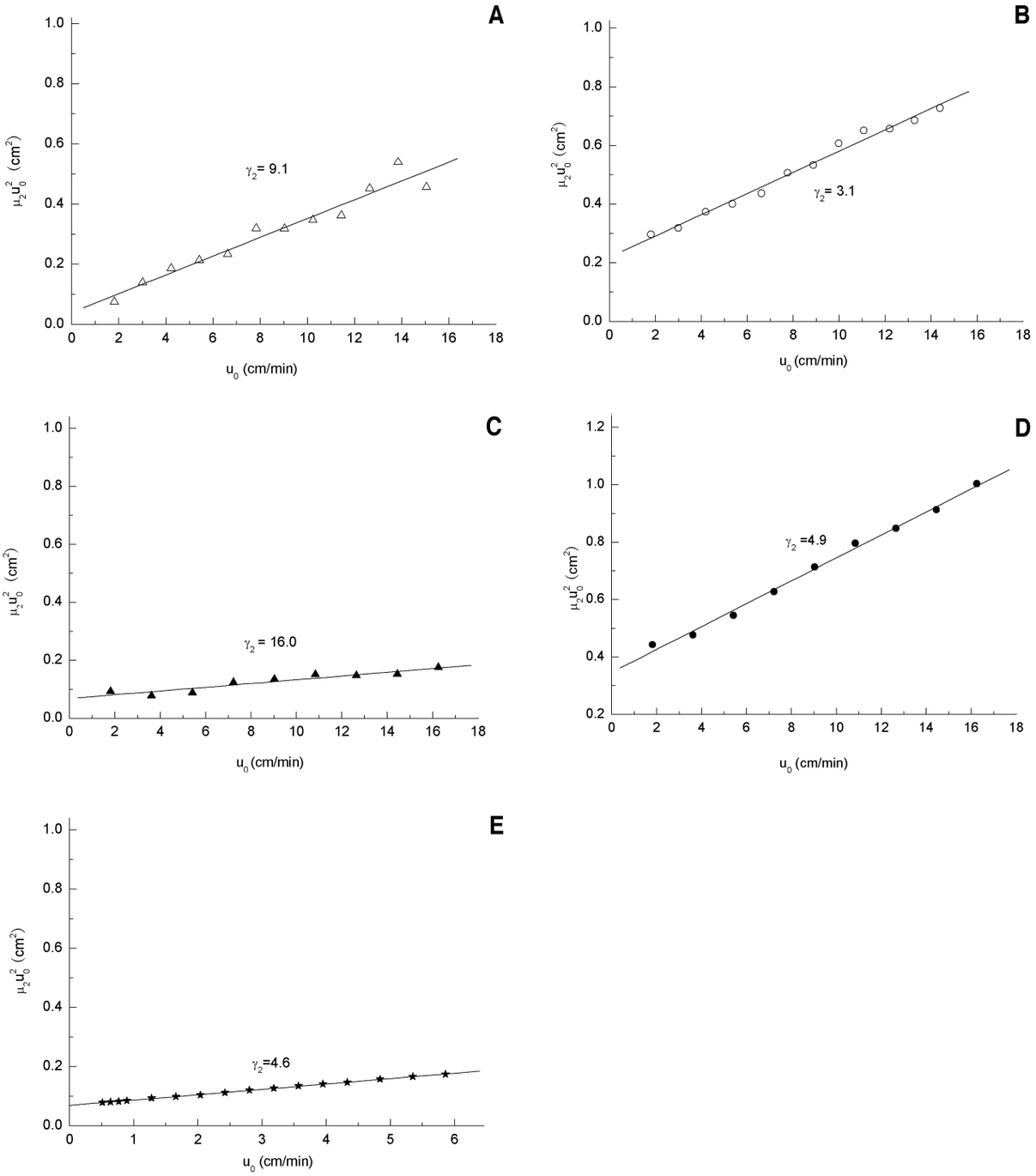

Figure 1. Plots of $\mu_2 u_0^2 \sim u_0$ obtained under conditions (A)–(E), respectively. A detailed description of the conditions is shown in Table I in the first part of this work.

Lin_aug2010_new.qxd:JCS template2 9/1/10 8:57 AM Page 5

Discussion about the result of third central moment

The experimental results of the third central moment in the first part of this work show that the linear correlation exists between $\mu_3 u_0^4$ and u_0. And now the result is discussed with the consideration of the moment equations of GR model earlier.

Based on Eq. 15–16, the following equation of $\mu_3 u_0^4$ can be deduced:

$$\mu_3 u_0^4 = 6\varepsilon_e D_L[\varepsilon_e + (1-\varepsilon_e)J] \cdot [\mu_2 u_0^2 - \frac{1}{12}\left(\frac{V_p}{\pi R^2}\right)^2 + L(1-\varepsilon_e)u_0^3\left(\frac{4R_p^4}{105D_{eff}^2} + \frac{4R_p^3}{15k_{ext}D_{eff}} + \frac{2R_p^2}{3k_{ext}^2}\right)J^3 \qquad \text{Eq. 19}$$

The experimental linear correlations of $u_3 u_0^4 \sim u_0$ indicate that the effect of the second right-hand side (RHS) term of the equation should be neglected, and the first RHS term of the equation should be approximately a linear function of u_0. Actually, the first RHS term of the equation is a quadratic function of u_0, according to the earlier analysis, but the datum in Table I [except for the result obtained under condition (A)] show that the linear part of this term is dominant. And this is the reason for the approximately linear experimental correlation between $u_3 u_0^4$ and u_0.

Although the quadratic part of the first RHS term of Eq. 19 is not dominant, it is significant because it is related to intraparticle mass transfer processes. To get more information about intra-particle mass transfer parameters, Eq. 16 is transformed to the style written below, in which the effect of the eddy diffusion is deducted to make the effect of intraparticle mass transfer resistances stand out:

$$\mu_3 u_0^2 - L\frac{12\varepsilon_e^2\gamma_2^2 dp^2[\varepsilon_e + (1-\varepsilon_e)J]^3}{u_0} = L \cdot 6\varepsilon_e\gamma_2 dp[\varepsilon_e + (1+\varepsilon_e)J]$$
$$(1-\varepsilon_e)\left(\frac{2R_p J^2}{3k_{ext}} + \frac{2J^2R_p^2}{15D_{eff}}\right) + Lu_0(1-\varepsilon_e)$$
$$\left(\frac{4R_p^4}{105D_{eff}^2} + \frac{4R_p^3}{15k_{ext}\cdot D_{eff}} + \frac{2R_p^2}{3k_{ext}^2}\right)J^3 \qquad \text{Eq. 20}$$

Table I. Linear Regression Parameters in Figure 1

	A* (cm²)	B* (cm · min)	$A^* - \frac{1}{12}\left(\frac{V_p}{\pi R^2}\right)^2$ (cm²)
Condition (A)	0.0398	0.0312	0.0386
Condition (B)	0.220	0.0361	0.219
Condition (C)	0.0690	0.0064	0.0678
Condition (D)	0.347	0.0399	0.346
Condition (E)	0.0695	0.0181	0.0694

* The values of A and B for each condition in Table I are equal to the intercept and slop, respectively, of the regression line in Figure 1.

The corresponding experimental correlations of:

$$\mu_3 u_0^2 - L\frac{12\varepsilon_e^2\gamma_2^2 dp^2[\varepsilon_e + (1-\varepsilon_e)J]^3}{u_0} \sim u0$$

can be obtained based on the measured results of the third central moment for conditions (C)–(E). They are shown in Figure 2A–2C, respectively, and the values of γ2 used here are from Figure 1. The corresponding results obtained under condition (A) and (B) are not shown here because of scattered data points caused by the poor measurement accuracy of the third central moments. The data points in Figure 2A appear

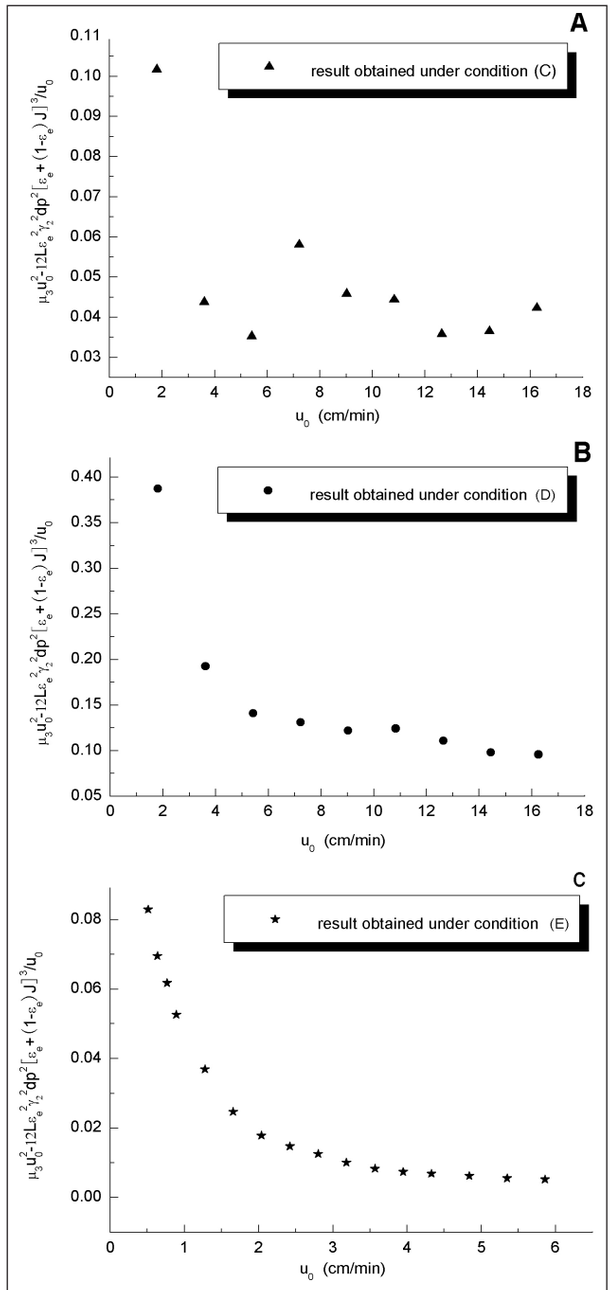

Figure 2. Plots of $\mu_3 u_0^2 - L\frac{12\varepsilon_e^2\gamma_2^2 dp^2[\varepsilon_e + (1-\varepsilon_e)J]^3}{u_0} \sim u_0$ obtained under conditions (A)–(E), respectively. A detailed description of the conditions is shown in Table I in the first part of this work.

Lin_aug2010_new.qxd:JCS template2 9/1/10 8:57 AM Page 6

scattered, and the regularity of the change of $\mu_3 u_0^2 - L\frac{12\varepsilon_e^2\gamma_2^2 dp^2[\varepsilon_e+(1-\varepsilon_e)J]^3}{u_0}$ with u_0 is not clear. But in Figure 2B, the drop tendency of the data points with increase of flow velocity can be found. And in Figure 2C, a clearer descending regularity is shown.

It can be concluded from the result of Figure 2 that the effect of the second RHS term of Eq. 20 is negligible, which is the same with the analysis result of Eq. 19. Furthermore, the decrease of $u_3 u_0^2 - L\frac{12\varepsilon_e^2\gamma_2^2 dp^2[\varepsilon_e+(1-\varepsilon_e)J]^3}{u_0}$ with u_0 shown in Figure 2 indicates the velocity dependence of the parameters in the first RHS term of Eq. 20. Among all the parameters involved in the term, the external mass transfer coefficient should be the most possible one, which is velocity-dependent and should increase with the flow velocity.

Now, based on the understanding of the velocity dependence of $k_{ext,}$ the correlation of $\mu_2 u_0^2 \sim u_0$ should be reconsidered. For the range of flow velocity in this work, Figure 1 shows that the experimental result of the second central moment always indicates the linear correlation between $\mu_2 u_0^2$ and u_0 under various experimental conditions. And as for Eq. 17, the most possible result ensuring that the linear correlation of $\mu_2 u_0^2 \sim u_0$ as well as the velocity-dependence of k_{ext} be valid simultaneously should be that k_{ext} is proportional to $u_{0.}$ And then with the effect of the molecular diffusion being neglected, Eq. 17 is rewritten as follows:

$$\mu_2 u_0^2 = \frac{1}{12}\left(\frac{V_p}{\pi R^2}\right)^2 + 2L\varepsilon_e\gamma_2 dp[\varepsilon_e + (1-\varepsilon_e)J]^2 + L(1-\varepsilon_e)\frac{2R_p J^2}{3\alpha} + Lu_0(1-\varepsilon_e)\frac{2R_p^2 J^2}{15D_{eff}} \quad \text{Eq. 21}$$

where α is the proportional coefficient (i.e., $k_{est} = \alpha \cdot u_0$). Obviously, the effect of the external mass transfer resistance is to contribute to the intercept of the regression line of $u_2 u_0^2 \sim u_0$, which is the same with the contribution of the eddy diffusion. This is why the larger values of γ_2 are obtained when the intercept of the regression line of $\mu_2 u_0^2 \sim u_0$ is attributed only from the eddy diffusion.

Discussion about the velocity dependence of k_{ext}

In fact, it is not a fresh conclusion that the external mass transfer coefficient k_{ext} is velocity-dependent. Numerous experimental investigations and a wide range of empirical mass transfer correlations for packed beds are available in the literature (14,22–30). Based on most of those correlations, the expressions of k_{ext} related to the flow velocity can be deduced. And the frequently used empirical mass transfer correlation by chromatography researchers is the Wilson-Geankolis correlation obtained at very low Reynolds numbers, which leads to an expression of k_{ext} proportional to $u_0^{1/3}$($k_{est} = \frac{1.09}{\varepsilon_e} u_0^{1/3}\left(\frac{D_m}{dp}\right)^{2/3}$) (31). Those expressions from various authors are different, especially of the exponent of the flow velocity, but they all indicate the positive correlations between k_{ext} and u_0.

On the other hand, the positive correlations between k_{ext} and u_0 can be explained by the physical origin of the external mass transfer resistance. When the mobile phase is flowing through the packing particles of column, the local flowing velocity is not uniform across the cross-section of the passage of the liquid because of the liquid viscosity. The local velocity is the highest in the center of the passage and is the lowest near the surface of the packing particles. Thus a boundary layer forms against the surface, which is normally named the stagnant film. The thickness of the boundary layer cannot be determined according to the theory of boundary layer because of the very low Reynolds range used in chromatography; but it is easy to understand that such thickness decreases with the increase of the flowing velocity of the mobile phase. And the external mass transfer coefficient reflects the difficult level for the solute molecular of traveling across the stagnant film through diffusion, as described by the equation $k_{ext} \approx \frac{D_m}{\delta}$, where δ is the thickness of the stagnant film. Therefore, with the increase of the flowing velocity, δ decreases and then k_{ext} increases. This is the explanation for the positive correlations between k_{ext} and $u_{0.}$

Determination of the parameters involved in GR model

Based on the analysis, the parameters in GR model are determined as follows.

Determination of the value of γ_2

The correlation of the axial dispersion coefficient (Eq. 18) was obtained from the experimental result of the column packed with nonporous glass balls, in which the geometric constant γ_2 is equal to 0.5. And the eddy diffusion is generally considered to originate from the non-uniform flow pattern around the packing particles in the column. It exists in the interstitial space among the packing particles. Therefore, the correlation obtained from the experimental result of the column of nonporous packing particles (Eq. 18) should be valid for the column packed with porous particles. And then, the value of γ_2 is still considered as 0.5 in this work.

In Figure 2, the plots of: $\mu_3 u_0^2 - L\frac{12\varepsilon_e^2\gamma_2^2 dp^2[\varepsilon_e+(1-\varepsilon_e)J]^3}{u_0}$ versus u_0 were calculated according to the measurement result of the third central moments using the values of γ_2 from Figure 1A–1E. Those γ_2 values are much larger than 0.5. It is easy to understand that the descending tendency of: $\mu_3 u_0^2 - L\frac{12\varepsilon_e^2\gamma_2^2 dp^2[\varepsilon_e+(1-\varepsilon_e)J]^3}{u_0}$ with the increase of u_0 does not change with the value alteration of γ_2. When the smaller γ_2 is used, the descending tendency of: $\mu_3 u_0^2 - L\frac{12\varepsilon_e^2\gamma_2^2 dp^2[\varepsilon_e+(1-\varepsilon_e)J]^3}{u_0}$ versus u_0 is more remarkable.

Determination of the values of k_{ext} and D_{eff}

And now, the values of k_{ext} and D_{eff} can be easily determined according to the linear regression of the experimental result of

Lin_aug2010_new.qxd:JCS template2 9/1/10 8:57 AM Page 7

the second central moment and Eq. 21. Because of the velocity dependence of $k_{ext,}$ only the proportional coefficient α of it is given. The result is shown in Table II.

Table II shows that the vales of the effective diffusivity D_{eff} of the phenylethane under conditions (B), (D), and (E) are similar, no matter the different mobile phases and columns that were used. And these values are larger than those of uracil under conditions (A) and (C). It is a reasonable result for two reasons. Firstly, it is because of their different chemical properties. Compared with uracil, the phenylethane is easier to dissolve in the mobile phases used in this work, and the molecular diffusivity of the phenylethane should be larger than that of uracil in these mobile phases. Secondly, as indicated by Eq. 10, the effective diffusivity consists of the pore diffusivity and the surface diffusivity. As for uracil, its intraparticle effective diffusivity is just the pore diffusivity for its non-adsorption property under the experimental conditions here. For phenylethane, besides the pore diffusivity the effective diffusivity also involves the effect of the surface diffusion, which has been reported (2–6) as an important contribution to the band broadening.

According to the value of 3α in Table II, it can be concluded that the external mass transfer coefficient of phenylethane is larger than that of uracil at the same flow velocity, which indicates the larger external mass transfer resistance of uracil. The result is consistent with the analysis of the smaller molecular diffusivity of uracil in the mobile phase used in this work.

The rationality of the values of D_{eff} and k_{ext} shown earlier is also a support for the conclusion of the linear velocity dependence of k_{ext}, which was developed earlier in this study. It indicates that those results obtained under the experimental conditions in this work are self-consistent. And what is more important is that the results show us a convenient method to determine the parameters involved in the GR model through the experimental result of the second central moment, which can be accurately measured; it is also a way to get more information about the mass transfer processes in the column. But the experimental condition taken in this work is still narrow, thus more experiments for different samples and mobile phases at wider ranges of flow velocity are needed for further discussion about the problem.

Conclusions

The experimental results of the second and third central moments are analyzed, combined with the moment equations deduced from the GR model. And it is concluded that under the experimental conditions in this work, the external mass transfer coefficient is dependent linearly on the flow velocity. Based on the conclusion, the reasonable values of the effective diffusivity and the external mass transfer coefficient are obtained.

Table II. Parameters Determined for Different Conditions

	D_{eff} (cm²/min)	3α
Condition (A)	7.98×10^{-7}	0.041
Condition (B)	4.98×10^{-5}	0.425
Condition (C)	3.87×10^{-6}	0.023
Condition (D)	4.51×10^{-5}	0.348
Condition (E)	5.31×10^{-5}	0.233

Acknowledgment

This work was supported by the fund of Group Project provided by Liaoning Education Department of China and the research foundation for Ph.D. Programs from Ministry of Education of China.

References

1. G. Guiochon, A. Felinger, A.M. Katti, and D.G. Shirazi. *Fundamentals of Preparative and Nonlinear Chromatography*, 2nd ed., Academic Press, Amsterdam, 2006.
2. K. Miyabe, A. Cavazzini, F. Gritti, M. Kele, and G. Guiochon. Moment analysis of mass-transfer kinetics in C_{18}-silica monolithic columns. *Anal. Chem.* **75:** 6975–6986 (2003).
3. K. Miyabe, S. Sotoura, and G. Guiochon. Retention and mass transfer characteristics in reversed-phase liquid chromatography using a tetrahydrofuran–water solution as the mobile phase. *J. Chromatogr. A* **919:** 231–244 (2001).
4. K. Miyabe and G. Guiochon. Kinetic study of the concentration dependence of the mass transfer rate coefficient in anion-exchange chromatography of bovine serum albumin. *Biotechnol. Prog.* **15:** 740–752 (1999).
5. K. Miyabe and G. Guiochon. Measurement of the parameters of the mass transfer kinetics in high performance liquid chromatography. *J. Sep. Sci.* **26:** 155–173 (2003).
6. K. Miyabe and G. Guiochon. Fundamental interpretation of the peak profiles in linear reversed-phase liquid chromatography. *Adv. Chromatogr.* **40:** 1–113 (2000).
7. K. Kaczmarski, D. Antos, H. Sajonz, P. Sajonz, and G. Guiochon. Comparative modeling of breakthrough curves of bovine serum albumin in anion-exchange chromatography. *J. Chromatogr. A* **925:** 1–17 (2001).
8. A. Cavazzini, K. Kaczmarski, P. Szabelski, D. Zhou, X. Liu, and G. Guiochon. Modeling of the separation of the enantiomers of 1-phenyl-1-propanol on cellulose tribenzoate. *Anal. Chem.* **73:** 5704–5715 (2001).
9. Z. Li, Y. Gu and T. Gu. Mathematical modeling and scale-up of size-exclusion chromatography. *Biochem. Eng. J.* **2:** 145–155 (1998).
10. T. Gu and Y. Zheng. A study of the scale-up of reversed-phase liquid chromatography. *Sep. Purif. Technol.* **15:** 41–58 (1999).
11. J.-H. Koh, P.C. Wankat, and N.-H.L. Wang. Pore and surface diffusion and bulk-phase mass transfer in packed and fluidized beds. *Ind. Eng. Chem. Res.* **37:** 228–239 (1998).
12. Z. Ma, R.D. Whitley, and N.-H.L. Wang. Pore and surface diffusion in multicomponent adsorption and liquid chromatography systems. *AIChE J.* **42:** 1244–1262 (1996).
13. C.R. Wilke and P. Chang. Correlation of diffusion coefficients in dilute solutions. *AIChE J.* **1:** 264–270 (1955).
14. E.J. Wilson and C.J. Geankoplis. Liquid mass transfer at very low Reynolds numbers in packed beds. *Ind. Eng. Chem. Fund.* **5:** 9–14 (1966).
15. H. Gao, X. Wu, and B. Lin. Application of Moment Analysis to Mass Transfer Kinetics of Reversed-Phase Liquid Chromatography:

Lin_aug2010_new.qxd:JCS template2 9/1/10 8:57 AM Page 8

Part 1. Experimental Investigation of Measurement of the Third Central Moment. *J. Chromatogr. Sci.* **48:** 478–483 (2010).
16. E. Kucera. Contribution to the theory of chromatography: linear non-equilibrium elution chromatography. *J. Chromatogr*. **19:** 237–248 (1965).
17. M. Kubin. Contribution to the theory of chromatography: influence of the diffusion outside and the adsorption within the sob-grains. *Collect. Czech. Chem. Commun*. **30:** 2900–2907 (1965).
18. M. Suzuki and J. M. Smith. Kinetic studies by chromatography. *Chem. Eng. Sci.* **26:** 221–235 (1971).
19. K. Miyabe and G. Guiochon. The moment equations of chromatography for monolithic stationary phases. *J. Phys. Chem. B* **106:** 8898–8909 (2002).
20. H. Guan and G. Guiochon. Study of physico-chemical properties of some packing materials: I. Measurements of the external porosity of packed columns by inverse size-exclusion chromatography. *J. Chromatogr. A* **731:** 27–40 (1996).
21. D.M. Ruthven. *Principles of Adsorption and Adsorption Processes,* John Wiley & Sons, New York, NY, 1984, chapter 7.
22. P.N. Dwivedi and S.N. Upadhyay. Particle-fluid mass transfer in fixed and fluidized beds. *Ind. Eng. Chem. Proc. Des. Dev*. **16:** 157–165 (1977).
23. T. Koloini, M. Sopcic, and M. Zumer. Mass transfer in liquid-fluidized beds at low Reynolds numbers. *Chem. Eng. Sci.* **32:** 637–641 (1977).
24. K. Rahman and M. Streat. Mass transfer in liquid fluidized beds of ion exchange particles. *Chem. Eng. Sci.* **36:** 293–300 (1981).
25. M. Bar-Ilan and W. Resnick. Gas-phase mass transfer in fixed beds at low Reynolds numbers. *Ind. Eng. Chem.* **49:** 313–320 (1957).
26. J.E. Williamson, K.E. Bazaire, and C.J. Geankoplis. Liquid-phase mass transfer at low Reynolds numbers. *Ind. Eng. Chem. Fund.* **2:** 126–129 (1963).
27. A.J. Karabelas, T.H. Wegner, and T.J. Hanratty. Use of asymptotic relations to correlate mass transfer data in packed beds. *Chem. Eng Sci.* **26:** 1581–1589 (1971).
28. J.D. Acetis and G. Thodos. Mass and heat transfer in flow of gases through spherical packings. *Ind. Eng. Chem*. **52:** 1003–1006 (1960).
29. L.K. McCune and R. H. Wilhelm. Mass and momentum transfer in a solid-liquid system. *Ind. Eng. Chem*. **41:** 1124–1134 (1949).
30. R. Pfeffer. Heat and mass transport in multiparticle systems. *Ind. Eng. Chem. Fund.* **3:** 380–383 (1964).
31. L. Hong, F. Gritti, G. Gulochon, and K. Kaczmarski. Rate constants of mass transfer kinetics in reversed phase liquid chromatography. *AIChE J.* **51:** 3122–3133 (2005).

Manuscript recieved February 28, 2009.